INTERNATIONAL JOURNAL FOR NUMERICAL METHODS IN FLUIDS, VOL. 5, 115–132 (1985)

A FINITE ELEMENT METHOD FOR THE SOLUTION OF TWO-DIMENSIONAL TRANSONIC FLOWS IN CASCADES

D. S. WHITEHEAD

Whittle Laboratory, Cambridge University Engineering Department, Trumpington Street, Cambridge, U.K.

S. G. NEWTON

Rolls Royce Limited, Derby, U.K.

SUMMARY

Steady two-dimensional transonic flow is calculated in cascades of compressor and turbine blades using a mesh of triangular finite elements. A velocity potential is used, the equations being solved by the Newton–Raphson technique. The resulting computer program is fast, and is shown to give good accuracy. Shock waves are well represented, provided they are not too strong.

INTRODUCTION

The aim of the work to be described in this paper is to calculate the steady flow in a cascade of compressor or turbine blades. The flow is assumed to be two-dimensional, except that a variation of the thickness of the stream surface will be allowed. The flow may be subsonic in some parts of the field, and supersonic in other parts, but will be assumed to be irrotational and isentropic, so that it is only possible to simulate shock waves with a small pressure rise across them.

Since the governing equations are non-linear, it appears to be necessary to use a field method in which the region of interest is covered by a mesh and numerical techniques are used. The most usual approach is to use a mesh of quadrilateral elements generated by two sets of lines, one set being straight lines in a tangential direction, and the other set approximating to the streamlines of a flow through the cascade. There are numerous references to work calculating the steady flow this way: for example the time-marching technique of Denton.[1]

The present work uses a mesh of triangular finite elements. This was chosen because it enables a large number of small elements to be packed into the regions of greatest interest, such as round the leading edges of the blades, with larger elements in regions where there is not much variation. The steady flow equations are then solved by the Newton–Raphson technique. This leads to a fast computer program but has the disadvantage that if a very large number of elements is used the computer storage requirement becomes very great.

The method has been extended to deal with small unsteady perturbations of the steady flow, so that the blade vibration problem can also be treated, and it is proposed to report this extension in a later paper. Another reason for choosing the Newton–Raphson technique for the steady flow is that it fits well with the unsteady calculation, since the unsteady calculation looks like one more iteration in the Newton–Raphson technique with different boundary conditions and complex variables.

0271–2091/85/02 0115–18$01.80

Received 9 November 1983
Revised 29 March 1984

Whitehead and Grant[2] have reported an earlier version of this work which is suitable for subsonic flow only. For supersonic flow this calculation becomes unstable. The calculation can be stabilized by using upwind densities, as has previously been found by many authors, for instance Deconinck and Hirsch.[3] The supersonic flow program is called FINSUP.

MESH GENERATION

An example of a mesh used for a compressor cascade is shown in Figure 1. The mesh covers an area one blade spacing in height, with one blade profile in the middle, and extends finite distances upstream of the leading edge plane and downstream of the trailing edge plane. The mesh generator starts from a specification of a number of points round the blade profile, which may be more closely spaced in regions of greater interest. These are then associated with a number of points round the boundary (the 'box') and corresponding points are joined by 'rays' as illustrated in Figure 2. The rays are usually single straight lines, but in the inlet and outlet regions they consist of two straight lines. The space between the rays is then filled in by triangular elements which are built up in layers round the blade profile, like the skins of an onion, the space between two adjacent rays in each layer being divided into two triangles. It is desirable to make the elements as nearly equilateral as possible, and to smoothly blend changes in element size to give optimum accuracy and convergence characteristics.

An important feature of the program is that the elements in the grid are renumbered (from the original construction) in order to reduce the bandwidth of the matrix involved in the flow calculation.

If the blade has a finite thickness at the trailing edge, then a cusp is added to simulate the separated flow which will in practice occur behind the trailing edge. The ray from this to the middle of the exit plane is drawn at the specified mesh outlet angle: a jump in potential occurs across this line, which models the wake.

In order to stabilize the calculation in supersonic flow it will be necessary to associate with each element an 'upstream' element. To do this accurately would require a knowledge of the direction of the steady flow, and this is not initially available. So the 'upstream' elements are assigned at the time of the mesh generation according to a rough rule. This is that for the regions between the rays

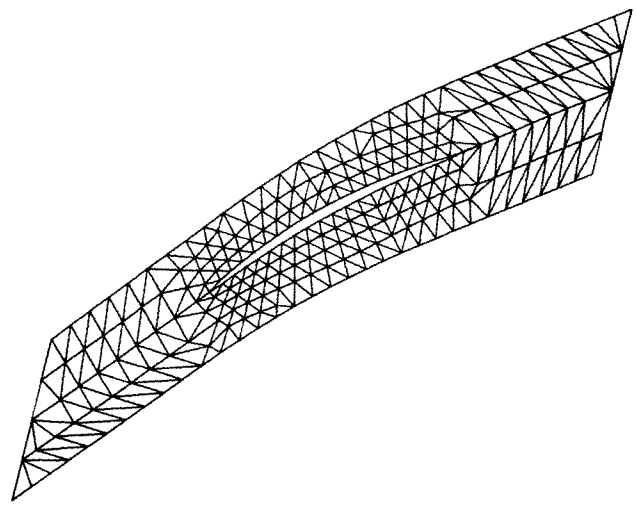

Figure 1. Typical finite element mesh

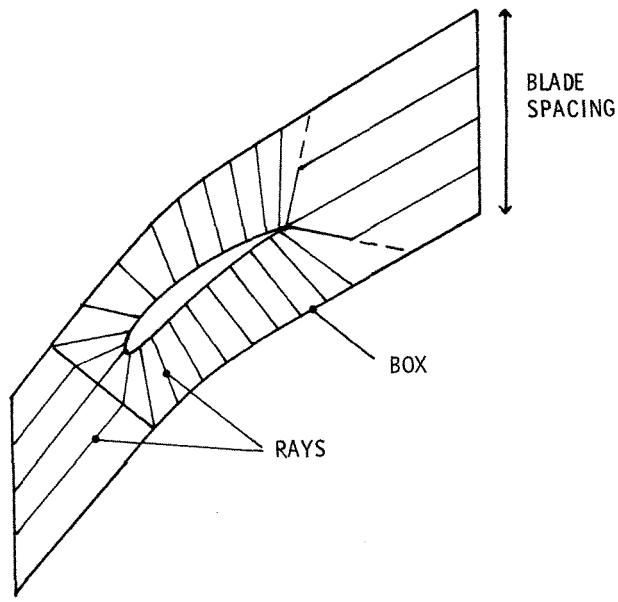

Figure 2. Construction of mesh

leading to the upstream and downstream faces, the flow is assumed to be along the channels between the rays. For the remaining regions, above and below the blades, the flow is assumed to be along the layers used in building up the elements.

STEADY FLOW EQUATIONS AND BOUNDARY CONDITIONS

The two-dimensional flow is assumed to be adiabatic, reversible and free from vorticity. Furthermore the fluid is treated as a perfect gas with no viscosity or thermal conductivity. It is therefore possible to define a velocity potential ϕ which is continuous in the solution domain apart from a jump across the wake line. Stream-tube radius variation and blade rotation are neglected, but stream-tube height (h) changes are included.

The differential equations governing the flow are mass conservation

$$\frac{\partial}{\partial x_i}(\rho h u_i) = 0 \tag{1}$$

and energy conservation

$$C_p T + \tfrac{1}{2}\mathbf{u}^2 = C_p T_0 \tag{2}$$

where the suffix 0 refers to stagnation conditions. The sound speed is given by

$$a^2 = \gamma R T \tag{3}$$

and hence

$$\frac{a^2}{a_0^2} = 1 - \left(\frac{\gamma - 1}{2}\right)\frac{\mathbf{u}^2}{a_0^2} = \left(\frac{\rho}{\rho_0}\right)^{\gamma - 1} \tag{4}$$

since the flow is isentropic. Together with the velocity potential

$$u_i = \frac{\partial \phi}{\partial x_i} \tag{5}$$

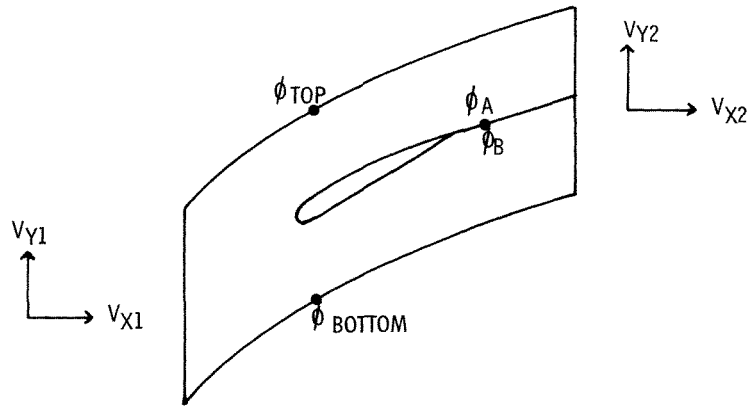

Figure 3. Boundary conditions

equations (1) and (4) form a set of non-linear equations for the two scalar functions ρ and ϕ.

The boundaries of the domain are illustrated in Figure 3. On the blade surface, the condition of no flow through the surface gives $n_i u_i = 0$. This means that in the finite element discretization (discussed in the next section) the blade surface is just like another element with no flow in it. No extra terms are required by this boundary condition, and it is therefore sometimes referred to as a 'natural' boundary condition. The cascade repeat condition gives, for corresponding points on the top and on the bottom of the domain,

$$\phi_{\text{TOP}} - \phi_{\text{BOTTOM}} = sV_{y1} \tag{6}$$

where V_{y1} is the inlet tangential velocity and s is the blade spacing. In addition, the condition that any flow leaving the top of the domain must be balanced by flow entering the bottom is satisfied.

The equations for the corresponding nodes on the top and bottom are added together to give an equation which is just like that for any internal node, except for the constant term on the right-hand side of equation (6).

The ray from the trailing edge, corresponding approximately in position to the wake from the blade, has a jump in velocity potential across it. This jump is equal to the anticlockwise circulation round the blade, and gives

$$\Delta\phi = \phi_{\text{B}} - \phi_{\text{A}} = s(V_{y2} - V_{y1}) = \Delta\phi_{\text{TE}}$$

Apart from this, the wake is treated like any other internal point, so that flow can cross the wake, but no flow is lost or gained. By making $\Delta\phi$ across the wake equal to $\Delta\phi$ at the trailing edge, the Kutta condition is automatically satisfied when the exit velocity is subsonic.

The choice of conditions which can be specified as input to the program requires some care. For supersonic inlet flow, when the cascade is not 'spilling', the inlet flow angle is determined by the blade geometry and inlet Mach number, so that the inlet flow angle is not a suitable input variable. For a choked cascade the flow is determined by the cascade geometry so that the total flow, or the inlet axial velocity, are also not suitable variables. The physical quantities which are effectively specified as input are therefore chosen as follows:

(a) inlet tangential velocity, V_{y1}
(b) stagnation density, ρ_0
(c) stagnation sound speed, a_0
(d) jump in potential between the bottom right corner of the mesh, and the bottom left corner of the mesh, $\phi_{\text{BR}} - \phi_{\text{BL}}$.

This last condition replaces the more physical condition of specified pressure rise through the cascade, which would determine the shock position for supersonic inlet flow of a real fluid with viscous effects and shock losses. For the idealized flow considered here, no specification of the inlet and outlet variables would fix the position of an in-passage shock in a cascade of flat plates at zero incidence. However the application of condition (d) determines the position of the shock uniquely.

In practice non-dimensionalization is carried out with respect to ρ_0 and a_0, and a scaled potential introduced which is zero at the bottom left and unity at the bottom right of the domain. This leaves as input the two variables

$$\mu_1 = u_{\mathrm{NOM}}/a_0$$
$$\mu_2 = V_{y1}/u_{\mathrm{NOM}} \tag{7}$$

where $u_{\mathrm{NOM}} = (\phi_{\mathrm{BR}} - \phi_{\mathrm{BL}})/\Delta s$ and Δs is the distance between the bottom left and bottom right corners of the box. This nominal velocity, u_{NOM}, does not have much physical meaning, except in the case of uniform flow through a cascade of flat plates, when it corresponds to the actual velocity. Incompressible flow solutions are obtained by setting $\mu_1 = u_{\mathrm{NOM}}/a_0 = 0$.

On the inlet face, the flow is matched to a linearized solution obtained by assuming that there are only small perturbations of the uniform flow far upstream. A similar treatment is applied on the exit face, but additional terms arise as a result of the jump in potential across the wake. Details of these inlet and outlet boundary conditions are not given here but are described by Whitehead.[4]

FINITE ELEMENT FORMULATION AND ITERATIVE SOLUTION

There are two aspects to the derivation of the discrete finite element equations corresponding to the differential flow equations given above. The first is to divide the solution domain up into elements and assume a prescribed variation of the unknowns over each element; the second is to obtain a series of simultaneous equations by multiplying the differential equation by each of a sequence of weighting functions, and integrating over the region. In the Galerkin method used here, the same 'shape functions' are used for both purposes. The very simple assumption of a linear shape function will be adopted here. Figure 4 shows a triangular element, with nodes numbered 1, 2 and 3. A general point within the element may be defined by the area co-ordinates Z_1, Z_2 and Z_3, where

$$Z_1 = A_1/A, Z_2 = A_2/A \text{ and } Z_3 = A_3/A \tag{8}$$

Here, A_1, A_2 and A_3 are the areas shown, and A is the total area of the element. Since

$$A_1 + A_2 + A_3 = A$$

it follows that

$$Z_1 + Z_2 + Z_3 = 1$$

Therefore only two area co-ordinates are independent.

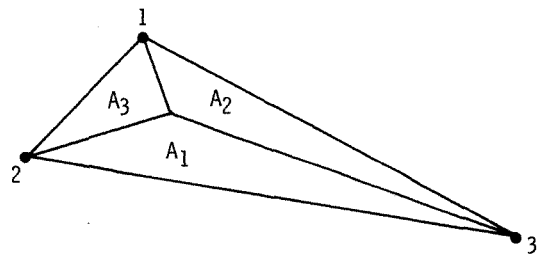

Figure 4. Area co-ordinates

The velocity potential ϕ is assumed to vary linearly within each element so that at any interior point

$$\phi = \phi_1 Z_1 + \phi_2 Z_2 + \phi_3 Z_3 = \phi_l Z_l \tag{9}$$

where Z_l is the shape function and ϕ_l gives the values of ϕ at the three nodes of the element. Contracted notation is employed here, so that summation over all three values of the repeated suffix l is implied.

The specific mass flow within the element is given by (10)

$$q_i = \rho h u_i$$

where

$$u_i = \frac{\partial \phi}{\partial x_i} = \phi_l \frac{\partial Z_l}{\partial x_i} \tag{11}$$

Since the problem is two-dimensional, i only takes the values of 1 and 2, corresponding to the x and y directions. Some analysis shows that

$$\frac{\partial Z_l}{\partial x_i} = \frac{1}{2A}\begin{bmatrix} (y_2 - y_3) & (y_3 - y_1) & (y_1 - y_2) \\ (x_3 - x_2) & (x_1 - x_3) & (x_2 - x_1) \end{bmatrix} \tag{12}$$

The equation of continuity (1) becomes

$$\frac{\partial q_i}{\partial x_i} = 0 \tag{13}$$

In order to satisfy this as accurately as possible within the finite element approximation, the Galerkin technique will be used. This equation is therefore multiplied by Z_l, producing three equations corresponding to the three values of l, and integrated over the element:

$$\int Z_l \frac{\partial q_i}{\partial x_i} \mathrm{d}A = 0 \tag{14}$$

This may be written

$$\int \frac{\partial}{\partial x_i}(Z_l q_i)\,\mathrm{d}A - \int q_i \frac{\partial Z_l}{\partial x_i}\mathrm{d}A = 0$$

in order to shift the differentiation from q_i to the 'well-behaved' shape functions. The first term may be transformed to an integral round the boundary of the element by Gauss' theorem giving

$$\int n_i q_i Z_l \,\mathrm{d}s - \int q_i \frac{\partial Z_l}{\partial x_i}\mathrm{d}A = 0 \tag{15}$$

where n_i is the unit normal drawn outwards from the surface of the element. Now consider all the elements adjoining a node L, as shown in Figure 5. Of the above three equations, the one corresponding to node L is picked out, and all such equations for the elements adjoining L are added to give

$$\sum_{\text{elements}} \int n_i q_i Z_l \,\mathrm{d}s - \sum_{\text{elements}} \int q_i \frac{\partial Z_l}{\partial x_i}\mathrm{d}A = 0 \tag{16}$$

In the first term, $n_i q_i$ is the flow across the boundary of the element. The area co-ordinate Z_l is zero over the sides of the element remote from L, such as AB. On a side such as AL, Z_l varies linearly from unity at L to zero at A. This term therefore expresses the flow disappearing down the

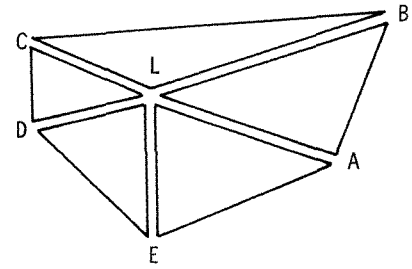

Figure 5. Elements adjoining node L

cracks meeting at L, weighted towards L. For the best representation of the continuity equation it must be put equal to zero.

In the second term the integral is uniform over each element. Hence

$$\sum_{\text{elements}} q_i \frac{\partial Z_l}{\partial x_i} A = 0 \tag{17}$$

Figure 6 shows the situation at the blade surface where the boundary condition $n_i q_i = 0$ is applied.

The natural procedure is now to substitute for q_i from equation (10). This leads to a program which is entirely satisfactory in subsonic flow, and has been described by Whitehead and Grant.[2] But in supersonic flow the process becomes numerically unstable, and if there is a patch of supersonic flow covering more than a very few elements the results are totally unrealistic. In order to overcome this problem use is made of 'upwind' densities. This device is well known and has been used for instance by Deconinck and Hirsch.[3] Equation (10) is modified to read

$$q_i = \{v\rho^* + (1-v)\rho\} u_i h \tag{18}$$

The * indicates an element upstream of the element under consideration and the artificial viscosity $v(M)$ will be defined in the next section.

From equations (11), (17) and (18)

$$\sum_{\text{elements}} \{v\rho^* + (1-v)\rho\} \phi_m \frac{\partial Z_m}{\partial x_i} \frac{\partial Z_l}{\partial x_i} hA = 0 \tag{19}$$

In view of the relationship (4) between density and velocity, equation (19) is a non-linear equation for the unknown values of ϕ_m. This will be solved by the Newton–Raphson technique. At any stage a current approximation to the solution is available which will be denoted by an overbar. The difference between this and the correct solution will be denoted by a prime, and it is assumed

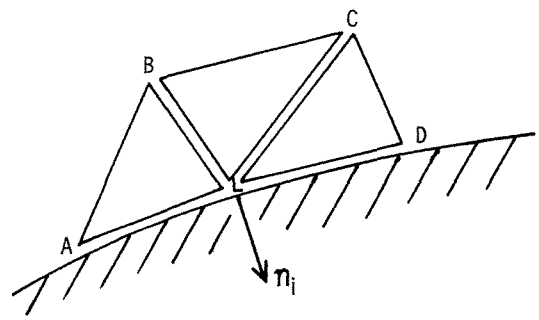

Figure 6. Elements at blade surface

that these correction terms are small. Hence

$$\begin{aligned} \phi &= \bar{\phi} + \phi' \\ \rho &= \bar{\rho} + \rho' \\ q_i &= \bar{q}_i + q_i' \end{aligned} \tag{20}$$

Neglecting terms of second and higher orders, the correction terms satisfy

$$\frac{p'}{\bar{\rho}} = \frac{a^2 \rho'}{\bar{\rho}} = -\bar{u}_j u_j' \tag{21}$$

Hence

$$\rho' = -\frac{\bar{\rho}}{\bar{a}^2} \bar{u}_j \frac{\partial Z_m}{\partial x_j} \phi_m' \tag{22}$$

Since the artificial viscosity is dependent upon Mach number, it is important to account for this in obtaining the perturbation to equation (19).

$$\nu' = \frac{\mathrm{d}\nu}{\mathrm{d}M} \frac{\mathrm{d}M}{\mathrm{d}u_j} u_j' = \frac{\mathrm{d}\nu}{\mathrm{d}M} \left(1 + \frac{\gamma - 1}{2} \bar{M}^2\right) \frac{\bar{u}_j u_j'}{\bar{M} \bar{a}^2}$$

where the derivative $\mathrm{d}\nu/\mathrm{d}M$ is taken at constant stagnation sound speed. Hence

$$\nu' = \frac{\mathrm{d}\nu}{\mathrm{d}M} \left(1 + \frac{\gamma - 1}{2} \bar{M}^2\right) \frac{\bar{u}_j}{\bar{M} \bar{a}^2} \frac{\partial Z_m}{\partial x_j} \phi_m' \tag{23}$$

Putting these results into the perturbation equation from (19) and rearranging gives

$$\sum_{\text{elements}} K_{lm} \phi_m' + \sum_{\text{elements}} K_{lm}^* \phi_m'^* + \sum_{\text{elements}} F_l = 0 \tag{24}$$

where

$$\begin{aligned} K_{lm} = {} & \{\nu \bar{\rho}^* + (1 - \nu)\bar{\rho}\} \frac{\partial Z_l}{\partial x_i} \frac{\partial Z_m}{\partial x_i} Ah - (1 - \nu) \frac{\bar{\rho}}{\bar{a}^2} \bar{u}_i \bar{u}_j \frac{\partial Z_l}{\partial x_i} \frac{\partial Z_m}{\partial x_j} Ah \\ & + \frac{\mathrm{d}\nu}{\mathrm{d}M} \frac{(\bar{\rho}^* - \bar{\rho})}{\bar{M} \bar{a}^2} \left(1 + \frac{\gamma - 1}{2} \bar{M}^2\right) \bar{u}_i \bar{u}_j \frac{\partial Z_l}{\partial x_i} \frac{\partial Z_m}{\partial x_j} Ah \end{aligned} \tag{25}$$

$$K_{lm}^* = -\frac{\nu \bar{\rho}^*}{\bar{a}^{*2}} \bar{u}_i \bar{u}_j^* \frac{\partial Z_l}{\partial x_i} \left(\frac{\partial Z_m}{\partial x_j}\right)^* Ah \tag{26}$$

$$F_l = \{\nu \bar{\rho}^* + (1 - \nu)\bar{\rho}\} \bar{u}_i \frac{\partial Z_l}{\partial x_i} Ah \tag{27}$$

The $\mathrm{d}\nu/\mathrm{d}M$ term is the additional term due to ν varying with M. In the calculation of ν and $\mathrm{d}\nu/\mathrm{d}M$, $\bar{M}$ is evaluated at the station (element) under consideration not at the upstream element as in some methods. The third term in equation (24) is the flow defect at node L for the current approximation, and is known. The functions K_{lm} and K_{lm}^* are also known, so that equation (24) is a linear set of equations for the unknown values of ϕ_m'. These equations are solved by simple Gaussian elimination, without any row or column interchanges, but taking advantage of the fact that the bandwidth of the left-hand-side matrix has been substantially reduced by the nodal renumbering scheme. By analogy with structural problems, K_{lm} and K_{lm}^* will be referred to as stiffness matrices. The analogy is that load corresponds to flow defect, and structural deflection corresponds to velocity potential.

ARTIFICIAL VISCOSITY AND CONVERGENCE

A survey of the literature indicates a variety of choices for $\nu(M)$:

(i) Deconinck and Hirsch[3]

$$\nu = \max\left\{0, \left(1 - \frac{1}{M^2}\right) M^n\right\}, \quad n \sim 4$$

(ii) Deconinck and Hirsch,[5] Jameson,[6] Hafez, South and Murman[7]

$$\nu = \max\left\{0, \left(1 - \frac{1}{M^2}\right)\right\}$$

(iii) Akay and Ecer[8]

$$\nu = \mu e\left(1 - \frac{1}{M^2}\right), \quad M \geqslant 1$$
$$= 0 \qquad\qquad M \leqslant 1$$

$\mu = 0{\cdot}3$, $0{\cdot}4$ or $0{\cdot}6$, and e is an integer which increases as one moves downstream from the sonic line in the supersonic region.

(iv) Holst[9]

$$\nu = \left(1 - \frac{\rho}{\rho_c}\right)^{\sigma}, \quad \sigma \sim 6$$

where ρ_c is the sonic density.

There are several factors to be considered in the choice of artificial viscosity:

(a) It must be high enough for stability of shocks and supersonic regions.
(b) It must be non-zero at $M = 1$ for stability of the iteration scheme.
(c) It should be as small as possible in subsonic regions for accuracy.
(d) It should be 'smooth' to avoid problems with the Newton–Raphson iteration scheme.

The role of artificial viscosity is to enable the use of the finite element method, which is an elliptic method, to solve a mixed elliptic/hyperbolic problem. It performs this feat by adding dissipation into the differential equation, or equivalently by biasing the scheme in the upstream direction.

Various forms of artificial viscosity were tried in the program on a variety of test cases, and the following form finally adopted:

$$\nu = \nu_0 + \nu_1\left(1 - \frac{1}{M^2}\right), M \geqslant 1 \tag{28}$$
$$\nu = \nu_0 M^{2\nu_1/\nu_0} \exp\left[-\lambda(M-1)^2\right], M < 1$$

These expressions give continuity of ν and $d\nu/dM$ at $M = 1$.

There are two choices of artificial viscosity (or damping) available to the program user:

$$\begin{aligned} &\text{Standard damping,} && \nu_0 = 0{\cdot}3, \quad \nu_1 = 1{\cdot}0, \quad \lambda = 20{\cdot}0 \\ &\text{High damping,} && \nu_0 = 0{\cdot}4, \quad \nu_1 = 1{\cdot}5, \quad \lambda = 1{\cdot}0 \end{aligned} \tag{29}$$

Figure 7 shows the variation of ν with Mach number for these two sets of parameter values. The fact that ν is non-zero for $M < 1$ contradicts the advice of many authors, e.g. References 3, 5–9. Furthermore $\nu > 1$ for some values of M, and this is contrary to the consensus of opinion. Numerical experiments have confirmed that (28) is a satisfactory choice of ν for a range of test

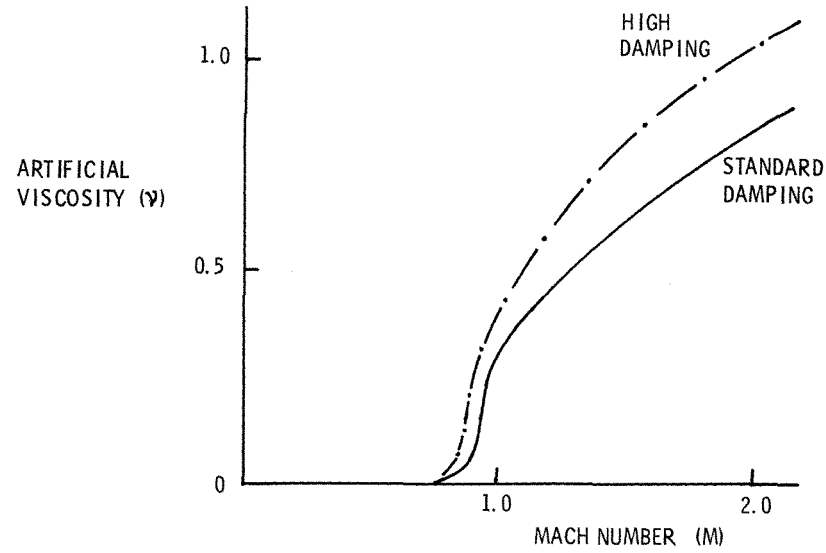

Figure 7. Variation of artificial viscosity with Mach number

problems. In order to enhance the convergence of the numerical scheme a large value of ν is used initially and this is gradually refined to the values of (29) as convergence is approached (following Akay and Ecer[8]).

High damping

Initial values:	$\nu_0 = 1{\cdot}0$,	$\nu_1 = 2{\cdot}0$,	$\lambda = 1{\cdot}0$
1st reduction:	$\nu_0 = 0{\cdot}67$,	$\nu_1 = 1{\cdot}58$,	$\lambda = 1{\cdot}0$
2nd reduction:	$\nu_0 = 0{\cdot}45$,	$\nu_1 = 1{\cdot}5$,	$\lambda = 1{\cdot}0$
3rd reduction:	$\nu_0 = 0{\cdot}4$,	$\nu_1 = 1{\cdot}5$,	$\lambda = 1{\cdot}0$

Standard damping

Initial values:	$\nu_0 = 1{\cdot}0$,	$\nu_1 = 2{\cdot}0$,	$\lambda = 20{\cdot}0$
1st reduction:	$\nu_0 = 0{\cdot}67$,	$\nu_1 = 1{\cdot}58$,	$\lambda = 20{\cdot}0$
2nd reduction:	$\nu_0 = 0{\cdot}45$,	$\nu_1 = 1{\cdot}25$,	$\lambda = 20{\cdot}0$
3rd reduction:	$\nu_0 = 0{\cdot}3$,	$\nu_1 = 1{\cdot}0$,	$\lambda = 20{\cdot}0$

Figure 8 indicates the rapid, if somewhat irregular, convergence obtained on a supersonic inlet case by using this technique.

The initial guess used for the Newton–Raphson iteration is based on uniform flow from bottom left to bottom right of the solution domain. For high-turning turbine blades this is not a very good approximation and the program was run with a low inlet Mach number to generate a better initial flow.

A further device has been used to stabilize the iterative scheme for difficult supersonic inlet cases, namely relaxation. Thus

$$\bar{u}_i^{(n+1)} = \bar{u}_i^{(n)} + Ru_i'^{(n)} \tag{30}$$

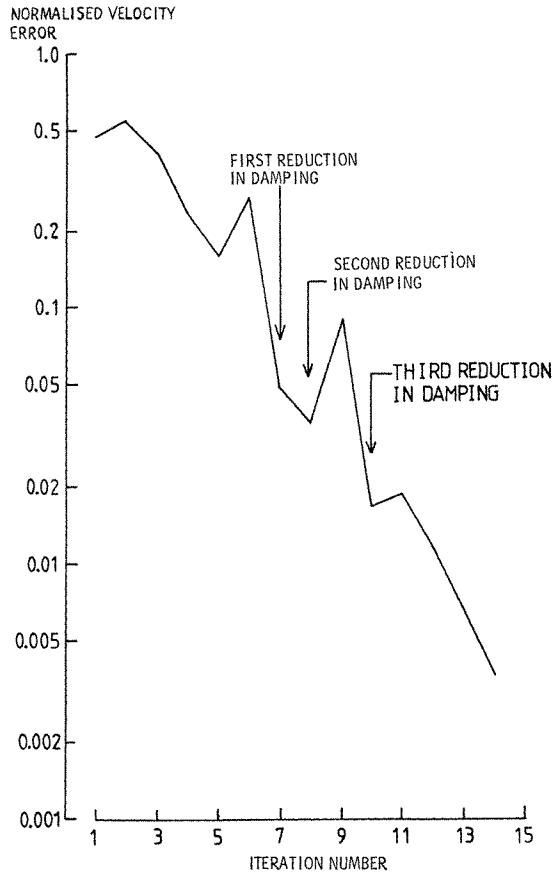

Figure 8. Typical convergence history

$0 < R \leqslant 1$ is the relaxation factor. Convergence of the iterative scheme is judged by tolerances on the changes in velocity and potential, considering the maximum change over all elements.

APPLICATIONS TO SUBSONIC AND TRANSONIC FLOWS

The following values are typical of the geometries used in the applications below:

Number of points around blade:	39
Inlet and exit distances:	0·8 × chord
Number of nodes:	300
Number of elements:	490

Figure 9 shows a comparison of FINSUP to a proven streamline curvature prediction method on a subsonic turbine stator, for a strictly two-dimensional flow. It can be seen that good agreement is obtained on this simple test case.

Next a blade with a transonic flow is considered. Figure 10 compares FINSUP predictions with measured blade surface Mach number for this turbine blade. The peak Mach number is approximately 1·1 and the Figure also includes a contour plot produced by the finite element

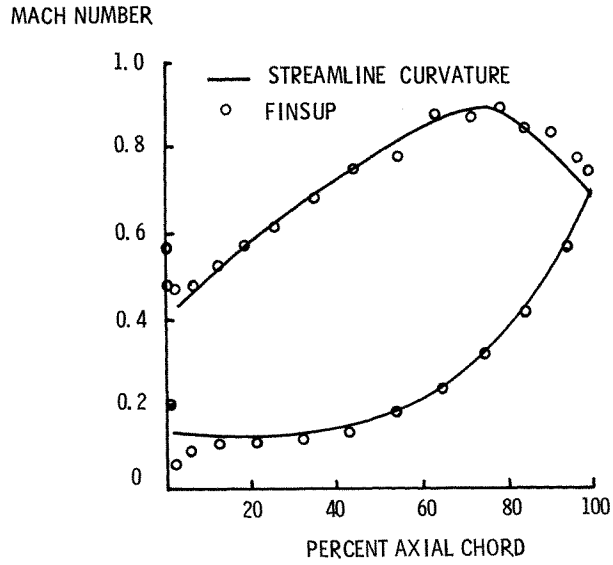

Figure 9. Subsonic turbine test case

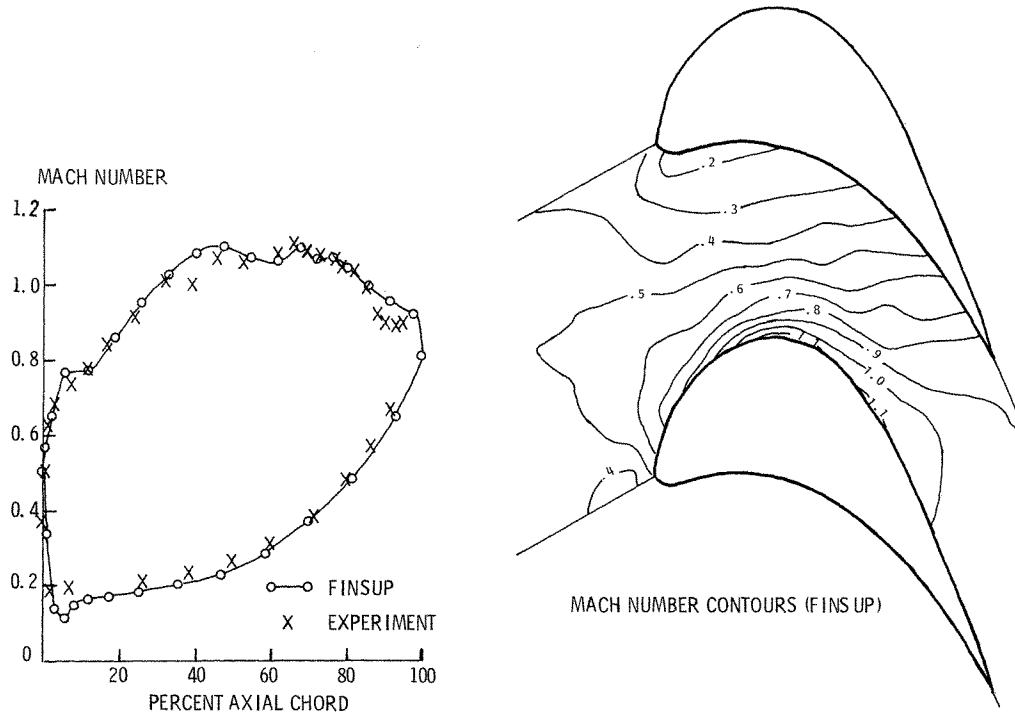

Figure 10. Comparison of FINSUP predictions with experimental data for ace blade

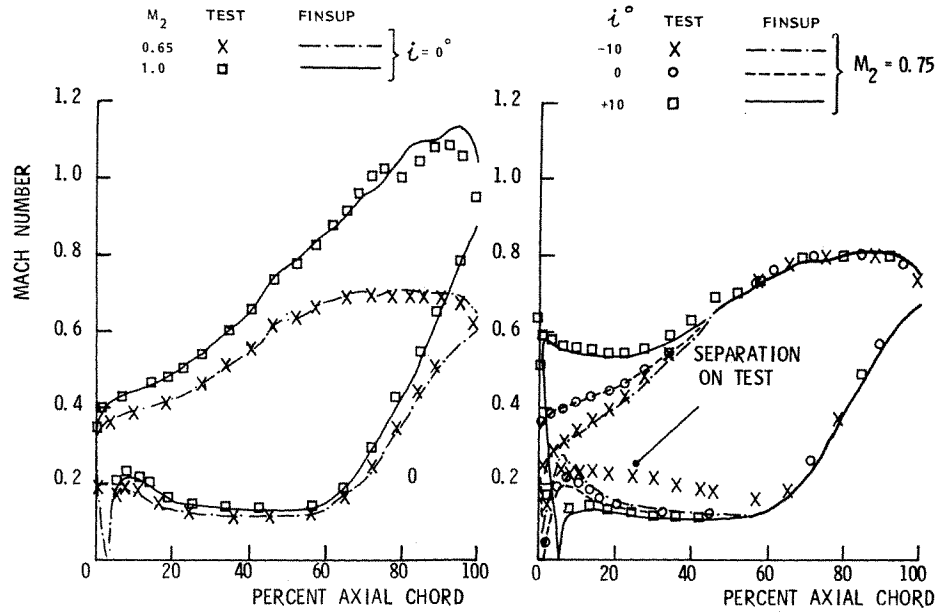

Figure 11. T7 comparisons with FINSUP

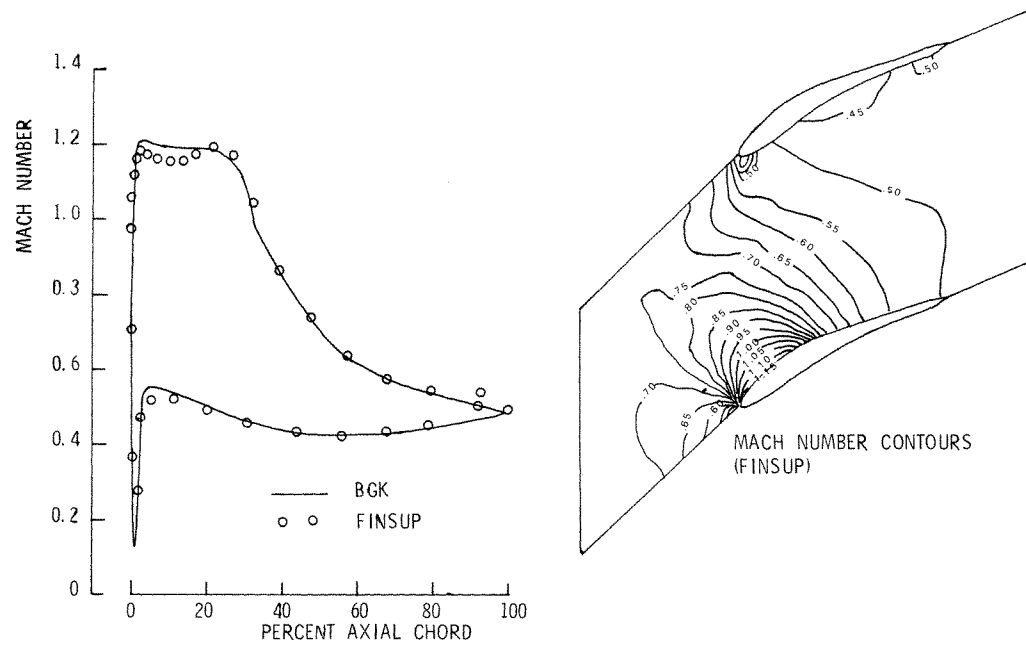

Figure 12. BGK supercritical test blade

program. (These contour plots are not very accurate owing to the interpolation procedures that are necessary. In particular they do not show an accurate repeat condition between top and bottom edges of these plots, whereas repeatability must in fact be exactly satisfied. Note that the calculations are performed in the domain of Figure 1, and that the blade-to-blade type domain is used merely for presentation of the Mach number contours.) A further comparison with experiment is shown for a different blade in Figure 11 for a range of exit Mach numbers and incidence conditions. The only significant discrepancy between experimental and predicted values is in a separated flow region where an inviscid method could not be expected to perform well.

The BGK (Bauer, Garabedian and Korn[10]) shockless supercritical blades are claimed to represent significant reductions in losses:[10,11] one obvious gain is that because they are so highly loaded, fewer blades are required and so a weight saving results. It is important to be able to analyse these blades in order to know whether or not they are sensitive to incidence changes and stream-tube height and radius effects. The aim here is to demonstrate that FINSUP is capable of treating such blades, with large supersonic patches and Mach numbers up to 1·2. Figure 12 shows the result of taking the geometry for the BGK test blade and calculating the flow using FINSUP. The slight discrepancy in the supersonic region is probably due to the very precise geometry definition required to give the 'correct' flow. Less than 50 points on the blade surface were used for the finite element calculation. A 3 per cent wake blockage was used in FINSUP to represent the open trailing edge of the BGK design: this was introduced by a linear reduction in stream-tube height over the last 30 per cent of blade chord. Thus there are two possible explanations for the discrepancy near the trailing edge:

(1) The blockage is not the same as the local effect of an open trailing edge.
(2) The finite element mesh is fairly coarse in this region.

SUPERSONIC INLET FLOW

The first supersonic flow case discussed is for a cascade of flat plates. The geometry used is that of Verdon and McCune Cascade A,[12] because this has been used for assessment of the unsteady part of the program also. The parameter values are:

Stagger = 59·53°
Space/chord = 0·7889
Inlet whirl velocity/stagnation sound speed = 0·9936

The steady flow solutions produced by FINSUP demonstrate the ability of the method to cope with supersonic inlet flow, and to predict 'shocks'. Figure 13 shows the effect on the solution of different amounts of artificial viscosity. Early versions of the program used fairly large constant values (e.g. $\nu = 1$ everywhere) and these led to a very smeared shock. Using the current version of FINSUP, with 'high damping' according to equations (28) and (29), the sharpness of the shock can be seen.

The above results were for $\mu_1 = 0{\cdot}9$, giving a shock near to the pressure surface leading edge. As μ_1 is varied the shock will move: increasing μ_1 drives the shock rearward and so loosely corresponds to reducing back pressure. Figure 14 shows the changes in inlet and outlet conditions as μ_1 changes. While the shock is within the passage no changes in M_1, α_1, M_2, α_2 occur—these conditions being those of unique incidence. As the shock is driven out rearward uniform flow is approached. By reducing μ_1 the shock can be made to stand off the blade pressure surface leading edge.

The next case considered is a 9·57° camber double circular arc (DCA) compressor blade (with a flat pressure surface) which was tested at DFVLR[13,14] under a range of conditions. The flow

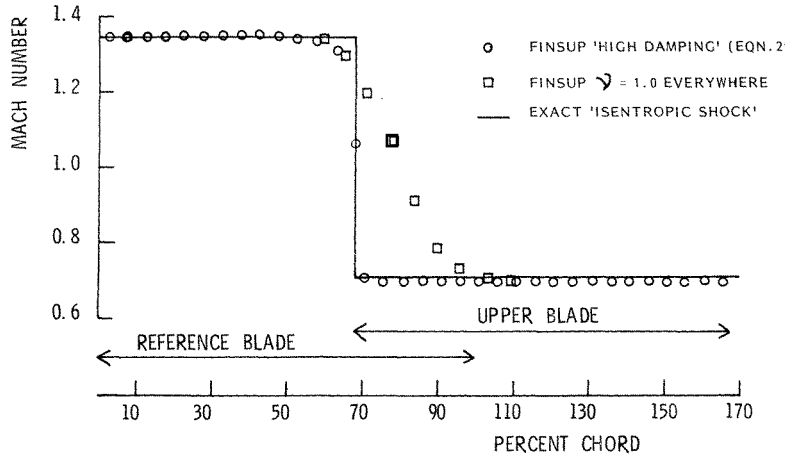

Figure 13. Effect of artificial viscosity on shock smearing

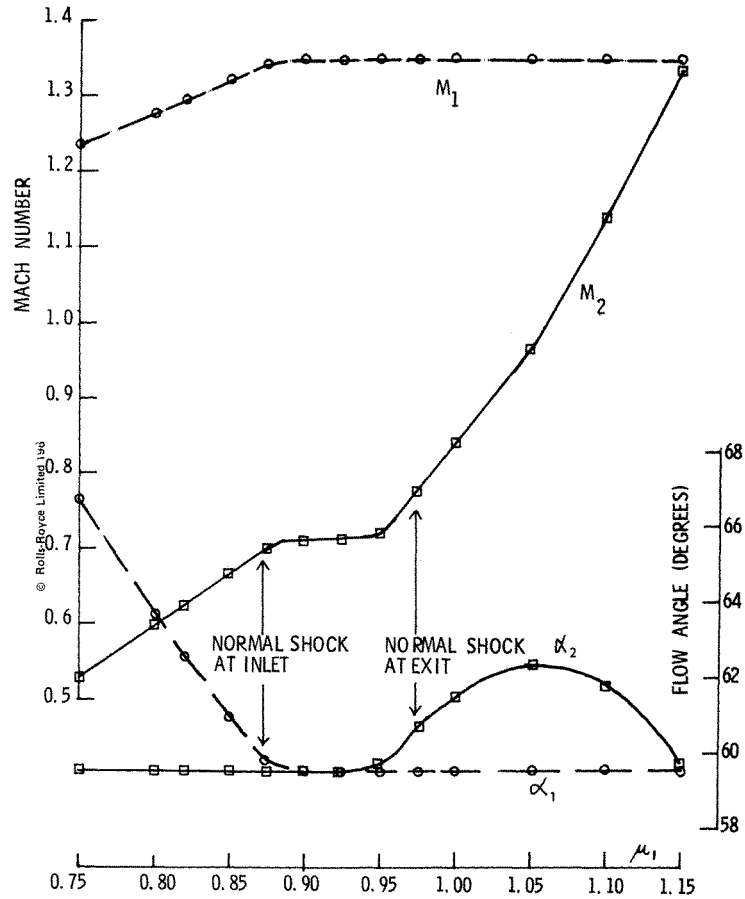

Figure 14. Variation with μ_1 for supersonic inlet case

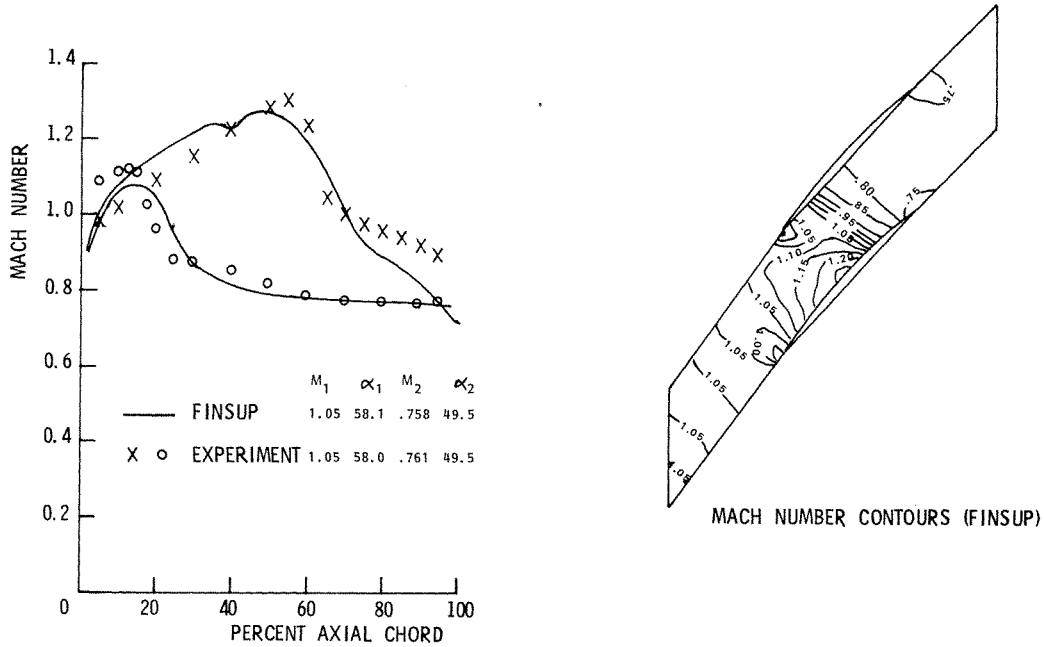

Figure 15. 9·57° DCA compressor at supersonic inlet

conditions used in this comparison are $M_1 = 1{\cdot}05$, $\alpha_1 = 58°$, $M_2 = 0{\cdot}761$, $\alpha_2 = 49{\cdot}5°$, $h_2/h_1 = 0{\cdot}86$ (linear from leading edge to trailing edge), which are the same values used by Deconinck and Hirsch.[3] M_1 and α_1 determine the inlet whirl and μ_1 is then adjusted to match the experimental outlet conditions. This creates a problem because as μ_1 ranges from 0·87 to 0·89, although the inlet and exit conditions hardly change, the surface Mach number and shock position alter significantly. Thus for this case there is a degree of ambiguity to the solution (as indeed for the flat plate case): this will only be resolved when a boundary layer and entropy increase at the shock are incorporated. It should be noted that the 14 per cent blockage allows FINSUP to match the experimental exit Mach number (isentropically), but the blockage is very much a global representation of the thick boundary layer behind the shock on the suction surface.

With these limitations in mind, Figure 15 shows experimental data against FINSUP predictions for $\mu_2 = 0{\cdot}87$ (which gives the shock in the correct position). Apart from the discrepancies behind the shock on the suction surface, the agreement is good, and those discrepancies can be attributed to boundary layer effects. Deconinck and Hirsch[5] give theoretical results for this blade which are very similar to those produced by FINSUP.

The final supersonic inlet example is a test blade devised by Calvert.[15] The section corresponds to about 60 per cent blade height for the fan of a typical civil high bypass ratio engine. Figure 16 shows a comparison between FINSUP and an (inviscid) time marching solution (based on Denton's method[1]) computed by Calvert[15] for a shock position near to the pressure surface leading edge. In order to obtain this solution by the finite element program it was found necessary to relax the iterative procedure using a relaxation parameter (R, equation (30)) of 0·5. The discrepancy between the two solutions on the pressure surface is because FINSUP has an isentropic calculation. The agreement on the suction surface is better than might be expected and there are two possible explanations for this. First the blade surface pre-shock Mach number calculated by FINSUP is slightly lower than the time-marching value, and this is countered by the fact that an

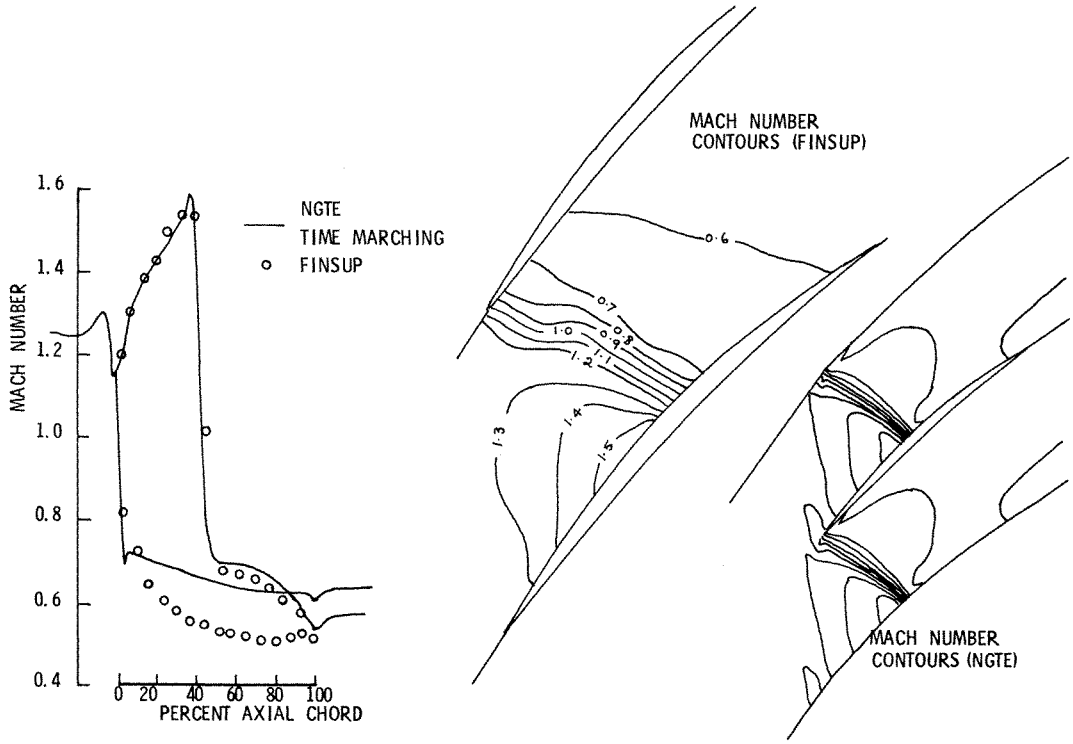

Figure 16. NGTE test blade with leading edge shock

isentropic solution will give a stronger 'shock jump'. Secondly, the finite element solution downstream of the shock may reflect more of an average of the preshock conditions, rather than that on the suction surface.

DISCUSSION

It is concluded that two-dimensional transonic flows in cascades can be predicted by FINSUP with acceptable accuracy. Furthermore the method is able to cope with blades with large supersonic patches, the so-called supercritical designs. For supersonic inlet flows with shocks the results are comparable with time-marching: the careful choice of artificial viscosity in FINSUP has led to a fairly robust method which does not exhibit shock 'overshoot' problems.

It has been demonstrated that the program can calculate the flow in a cascade of flat plates operating like tip sections of transonic fan blades in which the flow is 'spilling' round the leading edge and the unique incidence condition does not apply.

The program is fast enough to be interactive, owing to the use of the Newton–Raphson procedure (a full solution, including mesh generation and graphics and 14 iterations, taking typically 30 s cpu time on an IBM 370-168). The storage requirement is kept reasonable on account of the banded matrix techniques, each example given above using less than 20,000 values.

There are several areas in which development of the method would improve its performance and broaden the range of application.

(i) A more general variation of stream-tube height and the introduction of radius variation and rotation are essential for the method to be used on realistic quasi-3D flows.

(ii) Although the isentropic flow approximation is acceptable for mild shocks, as the pre-shock Mach number increases it becomes more desirable to allow for the entropy increase.
(iii) The inclusion of a boundary layer would greatly enhance the program's performance on many cases.

The first of these three developments is reported in Reference 16. It is important to realize that the latter two would not only increase the accuracy with which flows are predicted; they would also remove the uncertainty over shock position exhibited by inviscid, loss free solutions.

ACKNOWLEDGEMENT

Thanks are due to Dr. P. Stow for much helpful advice, and to G. Michel who performed the Figure 10 comparison. The authors are grateful to Rolls-Royce Limited for permission to publish this paper. Any views expressed therein are the authors' own and not necessarily those of the company.

REFERENCES

1. J. D. Denton, 'A time marching method for two and three dimensional blade to blade flows', *A.R.C.R. & M.*, 3775 (1974).
2. D. S. Whitehead and R. J. Grant, 'Force and moment coefficients for high deflection cascades', *Cambridge University Engineering Department Report*, CUED/A—Turbo/TR 98, May 1980.
3. H. Deconinck and Ch. Hirsch, 'Transonic flow calculations with finite elements', *GAMM Workshop 'Transonic flow calculations with shocks'*, Stockholm, September 1978.
4. D. S. Whitehead. 'The calculation of steady and unsteady transonic flows in cascades', *Cambridge University Engineering Department Report, CUED/A—Turbo/TR 118*, 1982.
5. H. Deconinck and Ch. Hirsch, 'Finite element methods for transonic blade to blade calculation in turbomachines', *ASME Paper No. 81-GT-5*, 1981.
6. A. Jameson, 'Acceleration of transonic potential flow calculations on arbitrary meshes by the multiple grid method', *Proceedings of the 4th AIAA Computational Fluid Dynamics Conference.*
7. M. Hafez, J. South, and E. Murman, 'Artificial compressibility methods for numerical solutions of transonic full potential equation', *AIAA Journal*, **17,** (8) (1979).
8. H. U. Akay and A. Ecer, 'Finite element analysis of transonic flows in highly staggered cascades', *AIAA 19th Aerospace Sciences Meeting, Paper No. 81-0210*, January 1981.
9. T. L. Holst, 'An implicit algorithm for the conservative, transonic full potential equation using an arbitrary mesh', *AIAA Paper 78-113*, 1978.
10. F. Bauer, P. Garabedian and D. Korn, 'Supercritical wing sections Volume III', *Lecture notes on economics and mathematical systems*, **150,** Springer-Verlag, 1977.
11. H. E. Stephens, 'Application of supercritical airfoil technology to compressor cascades: Comparison of theoretical and experimental results', *AIAA Paper 78-1138*, July 1978.
12. J. M. Verdon and J. E. McCune, 'The unsteady supersonic cascade in subsonic axial flow', *AIAA Paper 75-22*, January 1975.
13. F. A. E. Breugelmans, 'The compressor blade definition', *VKI Lecture Series 59: Transonic Flows in Turbomachinery*, May 1973.
14. F. A. E. Breugelmans and H. Starken, 'The cascade and rotor section performance of a 9.57° cambered DCA airfoil: comparison with 2D calculations in the transonic and supersonic flow regime', *VKI Lecture Series 59: Transonic Flows in Turbomachinery*, May 1973.
15. J. Calvert, Private Communication.
16. R. Cedar and P. Stow, 'The addition of quasi-three-dimensional-terms into a finite element method for transonic turbomachinery blade-to-blade flows', **5,** 101–114 (1985).